Proceedings of ASME Turbo Expo 2020
Turbomachinery Technical Conference and Exposition
GT2020
June 22-26, 2020, London, England

GT2020-15715

COMPARISON OF SODIUM SULPHATE DEPOSITION RATE MODELS BASED ON OPERATIONAL FACTORS INFLUENCING HOT CORROSION DAMAGE IN AERO-ENGINES

Evangelia Pontika[1], Panagiotis Laskaridis[1], Theoklis Nikolaidis[1], Max Koster[2]

[1]Cranfield University, Bedford, UK
[2]Lufthansa Technik A.G., Hamburg, Germany

ABSTRACT

Hot corrosion is defined as the accelerated oxidation/sulphidation in the presence of alkali metal molten salts. It is a form of chemical attack that causes good metal loss. Current lifing models in aircraft engines focus on creep, fatigue and oxidation while hot corrosion damage has been overlooked as being of secondary importance. However, the absence of hot corrosion lifing models for aircraft engines often leads to unexpected and unexplained hot corrosion findings by aircraft engine operators and Maintenance, Repair and Overhaul (MRO) providers during inspections. Although hot corrosion does not cause failure on its own, the interaction with other damage mechanisms can reduce component life significantly, consequently, there is a requirement for including hot corrosion in the damage prediction process of aircraft engines.

In both theoretical and experimental studies in literature, deposition of molten salts is identified as one of the primary conditions for hot corrosion to occur and an increased amount of deposited liquid salts accelerates the attack. Currently, most hot corrosion studies are limited to experimental testing of superalloys which are pre-coated with a controlled layer of salts. Such experimental studies are disconnected from gas turbine operating conditions during service.

The present paper analyses two deposition rate models applicable to gas turbine operating conditions using Design of Experiments. Design space exploration is presented by taking into account gas turbine operating parameters which vary during a flight as well as temperature ranges where hot corrosion can occur. Analysis of variance is presented for 6 input parameters using Box-Behnken 3-level factorial design. Results from the Analysis of Variance indicate that the deposition rate models are sensitive to pressure and salt concentration in the gas flow. Finally, the saturation point of sodium sulphate has been investigated within the operating range of gas turbine and it was found that it can vary significantly under different conditions.

Keywords: hot corrosion, deposition rate model, design of experiments

NOMENCLATURE

Symbols & Abbreviations

ANOVA	Analysis of Variance
C	Concentration
CL	Climb
D	Diffusion Coefficient
De	Descent
DoE	Design of Experiments
f	factor
h	Mass Transfer Velocity
HC	Hot Corrosion
HPT	High-Pressure Turbine
L	Length
La	Landing
Le	Lewis Number
LPT	Low-Pressure Turbine
MRO	Maintenance, Repair & Overhaul
MW	Molecular Weight
Na_2SO_4	Sodium Sulphate
NaCl	Sodium Chloride
Nu	Nusselt Number
P	Pressure
ppb	Particles Per Billion
ppm	Particles Per Million
R	Universal Gas Constant
Ri	Specific Gas Constant
St	Stanton Number
T	Temperature
TO	Take-Off
V	Gas Velocity
ΔH	Enthaply Change
ρ	Density
σ	Collision Diameter
Ω_D	Collision Integral for Lennard-Jones Potential

Indices

e	edge of the chemically frozen boundary layer
g	gas
i	species
m	mass
mol	mole fraction
s	surface
sat	saturation point
v	vapor
vap	vaporization
x	axial

INTRODUCTION

Current Status in Lifing Models

A significant factor in gas turbine engine development and through-life engineering services with regard to total life-cycle costs is the accurate prediction of engine life consumption and degradation due to operational life [1,2]. Current lifing models and studies for aircraft engines are focused primarily on creep and fatigue [2–6] and secondarily on oxidation, while hot corrosion effect has often been underestimated and overlooked [4]. This gap can result in unexpected and unexplained hot corrosion findings during engine inspections by Maintenance, Repair and Overhaul (MRO) providers and engine operators [7,8]. Although hot corrosion does not cause failure by itself, there is strong evidence that the presence of molten-salt hot corrosion and its interaction with other damage mechanisms can significantly decrease the overall life of superalloy components [9]. As a consequence of hot corrosion, the surface degradation and pitting of the attacked component promotes crack initiation [10], the material loss results in wall thickness loss reducing the load-bearing capability and, finally, the dissolution of the bond coat of gas turbines by the liquid salt deposits leads to faster thermal barrier coating failure. Engines which operate in coastal areas with high sea salt or polluted areas with sulfur oxides and sulfates are expected to suffer more hot corrosion [11,12], but currently, there is no physics-based methodology to quantify the damage prediction and compare different flight missions, flight segments and conditions.

Hot Corrosion Studies

Most hot corrosion rate studies are limited to experiments under specific, controlled lab conditions and aim at the evaluation of the hot corrosion resistance of the tested superalloy as a material itself, in most cases under atmospheric pressure and static air, and not as a component of a very complex engine. During such hot corrosion experiments [13–18], material scientists have conducted tests for specific gas temperatures, gas composition and a salt layer of pre-defined thickness, and by using advanced metrology techniques they calculated the good metal loss or mass gain due to hot corrosion attack. Subsequently, they plotted the results and in some of the studies [15,18] using curve fitting methods they extracted some formulas containing physics and empirical parameters in order to model hot corrosion rate for the specific conditions set and materials that they studied.

Although these models and conclusions have an undoubtedly important contribution towards understanding hot corrosion of alloys from the perspective of material science, they exhibit nearly no potential for direct application in gas turbine technology, aircraft engine degradation studies and maintenance scheduling. Such experimental studies do not investigate which combination of gas turbine conditions might lead to the selected pre-coated salt thickness or whether this salt layer evaporates during the experiment. It was only recently that Sumner et Al [19] highlighted the need for correlating the amount of the salts coating for the material testing with the potential of the deposits to evaporate/condense under the specified temperature, pressure and gas composition. Consequently, the present work is focused on filling the gap between the knowledge of the material behavior under controlled lab conditions with pre-coated specimens and the salt deposition propensity during real service conditions.

Hot Corrosion Theoretical Background

Hot Corrosion is a form of chemical attack which causes good metal loss. Hot corrosion has two types: 1. Type I (High-Temperature Hot Corrosion) in the temperature range of (800^{o} - 950^{o}C) and Type II (Low-Temperature Hot Corrosion) in the temperature range of 650^{o}C - 800^{o}C [20]. The dominant mechanisms are acidic fluxing and basic fluxing as thoroughly described in [21].

Type I Hot Corrosion

Type I Hot Corrosion is the high-temperature hot corrosion that takes place in the temperature range of 800-950^{o}C. The condensed molten salts dissolve first the protective oxide scale and then attack the substrate material [20]. The characteristic morphology of Type I Hot Corrosion is a uniform porous oxide layer and internal sulphidation [22].

Type II Hot Corrosion

Type II Hot Corrosion is the low-temperature hot corrosion that is observed in the temperature range of 650-800^{o}C. The reactions of type II hot corrosion are activated by high SO_3 partial pressure and the lower melting eutectics of Na_2SO_4-$NiSO_4$ for the nickel phase and Na_2SO_4-$CoSO_4$ for cobalt phase [23] with $NiSO_4$ being a corrosion product [24]. Low-temperature hot corrosion is localized and causes pitting crevices [25].

After reviewing hot corrosion theoretical and experimental studies [15,26–32], the most dominant parameters are identified: salt deposition, gas composition, temperature, material and presence of a coating.

Effect of Salts Deposition

As part of Simms et Al [33] experimental work on nickel superalloys, the deposition rate of a $(Na/K)_2SO_4$ salt mixture was varied within the range of 0-15μg/cm^2/h and an increase of good metal loss due to hot corrosion was observed with the increase of deposited salts under the same temperature. Sumner et Al [14], among the investigation of different exposure durations and salt

compositions, concluded that higher deposition fluxed was linked with higher hot corrosion rate on CMSX4 nickel superalloy. Deodeshmukh [34] also concluded that salt deposition rate has a high impact on the hot corrosion resistance of nickel superalloys, after conducting a series of experiments for different salt coatings. Therefore, salt deposition is a key factor and the calculation of the deposited salt is required for a hot corrosion damage investigation. Different deposition models and approaches are available in the literature. The current work assesses their suitability for adopting them in hot corrosion gas turbine studies based on operational factors.

Assessment of Component Conditions during Flight

Hot corrosion experiments on superalloy specimens are based on applying a controlled salt layer under atmospheric pressure and specific temperature, and the specimens are re-coated after a specific time. Such experimental studies do not consider the effects of varying gas flow conditions which are frequently met during gas turbine operation. Consequently, they do not assess the possibility of the salt layer being evaporated or how different pressures and salt concentrations in the gas flow might change and alter the saturation point of sodium sulphate. In the present study, the first step was an assessment of component conditions in-flight (Figure 1 and Figure 2) in order to identify which components and during which flight phases are more prone to hot corrosion based on the theoretical limits for hot corrosion type I, type II and oxidation. However, these theoretical limits do not specify if they refer to surface or gas temperature or both. The majority of hot corrosion experimental testing is conducted on non-cooled specimens which are in thermal equilibrium with the gas environment. In reality, in gas turbines there are both cooled and non-cooled components and the issue of how a difference between surface and gas temperature affects the phenomenon remains unclear in literature. This issue was observed in this study, consequently both surface and gas temperature are going to be assessed in this preliminary analysis since there is no definite conclusion in the literature. The view of the authors is that surface temperature is expected to have a more direct impact on hot corrosion rate since it involves surface reactions, however gas temperature has an indirect effect by influencing salt evaporation/condensation.

The case used for the current analysis is an engine model similar to CFM56-7B engine in terms of configuration and thrust level, during a representative 4-hour flight mission of an aircraft model similar to Boeing 747-800. The flight mission analysis was executed in HERMES, an in-house aircraft performance tool at Cranfield University, and for the engine performance simulation Turbomatch was used, an also in-house engine performance simulation tool [35].

Take-Off Weight	71031	[kg]
Cruise Altitude	10668	[m]
Cruise Mach	0.785	-
Duration	4.092	[km]
Range	3052	[km]

TABLE 1: FLIGHT MISSION PARAMETERS

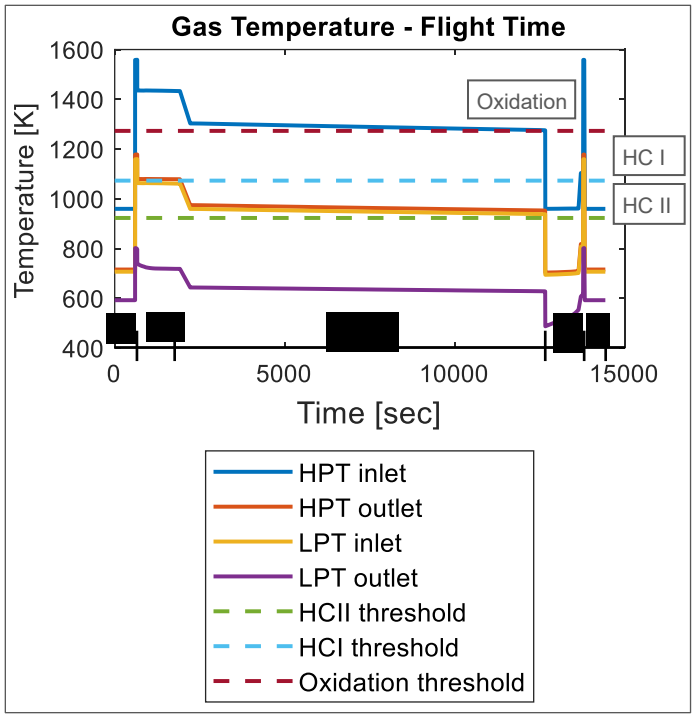

FIGURE 1: GAS TEMPERATURE OVER FLIGHT TIME AND HOT CORROSION RANGE

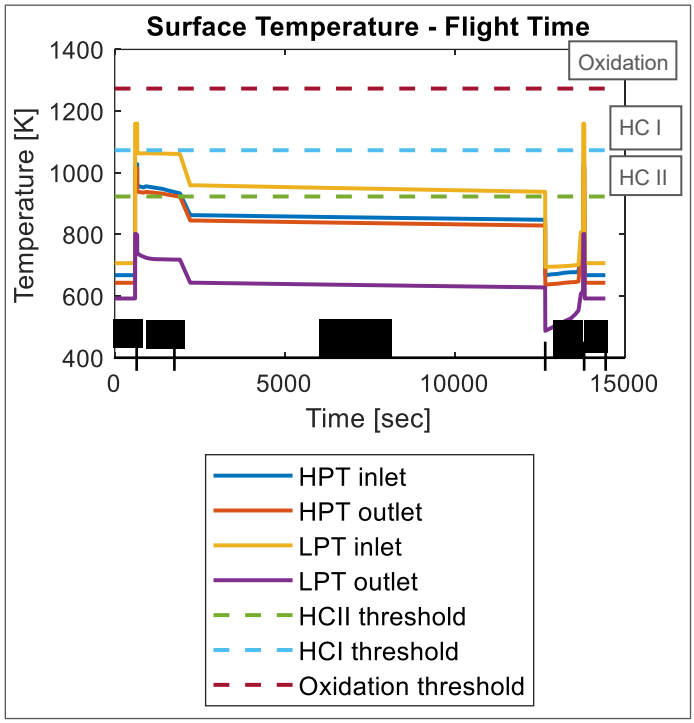

FIGURE 2: SURFACE TEMPERATURE OVER FLIGHT TIME AND HOT CORROSION RANGE

Figure 2 indicates that HPT inlet, HPT outlet and LPT inlet surface temperatures are within the theoretical temperature range for Hot Corrosion to occur.

Figure 1 indicates that the HPT inlet gas temperature is within the hot corrosion range only during taxi-out, descent and taxi-in, while for take-off, cruise and landing it is above the temperature limit further which oxidation is the dominant chemically induced mechanism. HPT outlet and LPT inlet conditions are favorable for Hot Corrosion to occur, while LPT outlet has too low temperature for Hot Corrosion to begin. Intermediate LPT stages are expected to be in the temperature range for Hot Corrosion.

However, Figure 1 and Figure 2 only assess components based on the theoretical limits of hot corrosion. A more thorough analysis adjusted to how the different operating conditions in-service can affect the evaporation threshold is required for more accurate deposition rate studies and par-extension more accurate hot corrosion lifing prediction. Saturation temperature variation during the same flight mission will be presented in the results section.

METHODOLOGY

Review on Deposition Rate Approaches

In recent literature, many deposition studies have focused on high fidelity particle tracking methods using numerical tools [36–39] or particle rebound conditions based on their diameter [40]. Guha has extensively reviewed deposition using particle tracking [37]. Forsyth [39] proposed a dynamic mesh method which accounts for the change of geometry due to thick layers of deposited particles and it mostly applicable to large particles such as sand.

However, for hot corrosion lifing investigations that aim at predicting the overall propensity for salts deposition on a component surface during thousands hours of operation, high fidelity methods using particle tracking are not applicable as there is uncertainty in many boundary conditions and complexity increases. Apart from the lack of boundary conditions and geometrical details about the particles, the aforementioned high fidelity methods require tuning of parameters for the specific application and particle type to match experimental results if available. There are basic unknown parameters, such as inlet particle trajectories and particle size, consequently lower fidelity, analytical models that use operational parameters have better applicability and reduced complexity. In the present analysis, a more thermodynamic approach is selected, by checking the condition for condensation/evaporation and then applying a deposition rate model which correlates sodium sulphate deposition rate with gas turbine operating conditions. The models ([18,41,42]) used in this work are still based on experimental studies, include non-dimensional coefficients for heat transfer and flow characteristics and have their own limitations, but the produced formulas are generalized and can be applied over a range of operating conditions after calculating the required physical properties without the need for further experiments to tune empirical factors. In search of analytical models for deposition/condensation calculation based on physical properties and relations, potential models were found in [15,18,41,42]. In the current paper two analytical models, one based on the chemical frozen boundary layer theory [41,42] and another based on mass transfer velocity [18], which both had comparable values and physics, were selected to be analyzed.

However, the deposition rate models do not take into account that above the saturation point of sodium sulphate – which is a combination of temperature and pressure – evaporation begins. Under the highly varying operating conditions in gas turbine components, the range that condensation can take place has to be identified for a complete study. The threshold for condensation/evaporation to begin is the saturation point.

For the specific pressure and Na_2SO_4 concentration [43] at every operating point, saturation temperature is calculated and the following condition has to be checked:

- If $T > T_{sat} \rightarrow$ evaporation
- If $T < T_{sat} \rightarrow$ condensation

This is the general condition that applies to all evaporation/condensation problems. Ahluwalia et al [18] distinguished 3 different cases of cooled gas turbine components and sodium sulphate deposition:

- If $T_s < T_{sat}$ and $T_g >> T_{sat} \rightarrow$ evaporation
- If $T_s < T_{sat}$ and $T_g \geq T_{sat} \rightarrow$ condensation
- If $T_s < T_{sat}$ and $T_g < T_{sat} \rightarrow$ condensation

Deposition Rate Model 1

The first model under investigation is based on the chemically frozen boundary layer theory, which appears in [41,42,44–46]. The mass transfer of sodium-containing species i to the component wall is calculated using Equation 1 and then the assumption that all sodium which reaches the wall is converted to sodium sulphate is made to calculate the total mass transfer of sodium sulphate onto the component wall.

$$\dot{m}_{i.s} = F(turb) \cdot \left\{ \frac{(D_i \rho)_e}{L} \cdot F_i(soret) \cdot Nu_{m,1} \cdot \left[(C_{i.e} - C_{i,s}) + \tau_i \left(\frac{F(ncp)}{F_i(soret)} \right) \cdot C_{i,s} \right] \right\} \quad (1)$$

F(turb) and F(ncp) are correction factors that account for turbulence and non-constant properties respectively, but the default value 1.0 can be used. F(Soret) is a correction factor for Soret diffusion and can be approximated as a function of effective thermal diffusion factor as described in [42,47]. D is the diffusion coefficient of the species, ρ is the density, L is the blade length and $C_{i,e}$ is the species concentration at the edge of the chemically frozen boundary layer, $C_{i,s}$ is the concentration of species near the wall and τ_i is the thermal diffusion factor. This model is based on Fickian diffusion, corrected with the aforementioned correction factors to account for extra effects.

The authors in [41] tested their theory against experimental data from a NASA test rig in the temperature range of 1100-1300K, under atmospheric pressure and for concentration of Na_2SO_4 10.5ppm. They noticed over-predictions when surface temperature was near the dew point temperature (around 1157K) but they discuss that overall the model makes reasonable predictions for vapour and small particles and for temperatures not far below the dew point, when nucleation effects begin.

Deposition Rate Model 2

Ahluwalia et Al [18] described the mechanism for Na_2SO_4 condensation onto a cooled surface of a coal-fired gas turbine and proposed a simple calculation using mass transfer velocity and difference of partial pressures in the gas phase and near the surface:

$$\dot{m}_i = \frac{h_{m,i}}{R_i T_s}\left[P_{v,i}(T) - P_{sat,i}(T_s)\right] \quad (2)$$

$H_{m,i}$ is defined as the mass transfer velocity of species i to the component wall and is correlated with gas velocity, Stanton number St and Lewis number Le:

$$h_{m,i} = V \cdot St \cdot Le_i^{-\frac{2}{3}} \quad (3)$$

Ahluwalia et al applied this model [18] for Tw=700-1300K, T_g=1300K and 1500K and for sodium concentration 0.1=10ppm. They observed that condensation is allowed when wall temperature is below the dew point of Na_2SO_4 but gas temperature is not much higher than the dew point. They also note that when both gas temperature and surface temperature are far below the dew point of sodium sulphate, nucleation of sodium sulphate vapor takes place and thermophoretic transport becomes the driving mechanism for condensation so extra considerations must be made.

Threshold for Evaporation/Condensation

In the current work the applicability of the deposition rate models is limited by the saturation point of sodium sulphate under the specific conditions. Antoine equation is an extension of the Clausius-Clapeyron equation and describes the relation of saturated vapor pressure and temperature [48]. Clausius-Clapeyron equation allows calculation of vapor pressure at another temperature if vapor pressure is known at another temperature.

$$\ln P = \frac{\Delta H}{RT} + c = \ln\frac{P_1}{P_2} = \frac{\Delta H_{vap}}{R}\cdot\left(\frac{1}{T_1} - \frac{1}{T_2}\right) \quad (4)$$

Studies calculating the enthalpy of vaporization of Na_2SO_4 are reviewed in [49]. Equation 4 can be written in the semi-empirical form of Equation 5 which is used to fit experimental data and it is called Antoine equation [50]. The derivation is described in [51].

$$\log_{10} P = A - \frac{B}{T - C} \quad (5)$$

P is the saturated vapor pressure and T the corresponding saturation temperature. A, B, C are constants which are experimentally defined for a specific temperature range and species.

When saturation temperature is investigated for a known pressure then P in Equation (5) is the partial pressure of the depositing species in the gas phase:

$$P_i = C_{mol,i} \cdot P_g \quad (6)$$

Where $C_{m,i}$ is the mole fraction of species i in the gas and P_g is the gas total pressure. P_i is substituted in Equation 5, which is subsequently solved for saturation temperature T.

Above the saturation point, the mass transfer mechanisms must be integrated with an evaporation model to calculate the remaining salt layer on the component surface.

Design of Experiments

Design of Experiments (DoE) is a systematic way to observe the response of a system's output to the variation of input variables. In the present work, DoE 3-level (3^k) fractional factorial design method was used to understand the sensitivity of the deposition rate models to different gas turbine operating conditions and salt contamination. Fractional factorial design is an efficient way to study a system that involves two or more factors by creating blocks of different combinations of factor levels. The three levels in the 3^k design are low, intermediate and high. In the present study, Box-Behnken design [52] has been used to generate the variable blocks. Full 3-level factorial design, which includes all possible combinations of factor levels, was also investigated and compared with the Box-Behnken design results, and the conclusions were in agreement. However, only Box-Behnken design results will be presented in this paper as a more efficient method which requires less runs. There are more available design methods in literature but analyzing all of them and optimizing DoE is out of the current scope.

Variable Limits

First, the design space was defined by setting the value range for the input variables (Table 3). Sea salt consists of [53]:

Compound	Wt%
NaCl	58.49
Na_2SO_4	9.75

TABLE 2: SODIUM-CONTAINING SPECIES IN SEA SALT

Sea salt concentration in the air is within the range of 0-22 [ug/m^3] [54] = 0-17.96 [ug/kg$_{air}$]=0-17.96 [ppb]. By combining the information from Table 2 the design variable limits of NaCl concentration and Na_2SO_4 concentration are set in Table 3. For the selection of the upper limit for Na_2SO_4 concentration, the possibility of full conversion of NaCl to Na_2SO_4 has also been considered. The blade and gas temperatures under investigation should be within the temperature range of hot corrosion. Finally, gas axial velocity and pressure are within the typical range for gas turbine components.

No	Variable	Lower Limit	Upper Limit	Units
1	C_{NaCl}	0.0001	11	[ppb]
2	C_{Na2SO4}	0.0001	35	[ppb]
3	V_x	150	300	[m/s]
4	P	1	30	[atm]
5	T_g	900	1300	[K]
6	T_b	900	1300	[K]

TABLE 3: INPUT VARIABLE LIMITS – DESIGN SPACE

Analysis of Variance

Analysis of Variance means that the total variability of the model is analyzed to the effect of its component variables. The calculation of the required squared differences are thoroughly described in [55]. The result of the analysis of variance is the F ratio, which is a factor expressing the ratio of the variability between samples and variability within samples [55].

Finally, the F ratio of each variable is compared with the critical value of F. Prob>F as in the last column of the ANOVA tables (Table 4, Table 5) expresses the probability that the variable confirms the null-hypothesis. Lower probability to confirm the null hypothesis means that the variable is more significant.

In this study, all variables were considered independent. This means that the gas temperature and surface temperature are varied independently to assess the models' response to each of the variables individually and thermal analysis is not included to correlate surface temperature with gas temperature. Taking into consideration all the possible surface-gas temperature combinations that may occur in engines of different level of technology, different components, different spatial locations of the components, different flight phases as well as the existence of transient states, the choice of not including a surface thermal analysis does not constitute a limitation. This is a deposition rate model sensitivity analysis using typical gas turbine operating conditions, consequently it should not be narrowed to a specific case of engine, component and flight phase, hence specific cooling model and surface-gas temperature codependence. Finally, the analysis of variance and creation of the factorial design were processed using MATLAB [56] tools for DoE.

RESULTS AND DISCUSSION

Saturation Point Variation

By using Equations 5-6 for a typical pressure range in aircraft engine components and the design limits for Na_2SO_4 concentration (Table 3), Figure 3 is obtained and it demonstrates the variation of saturation temperature in the design space.

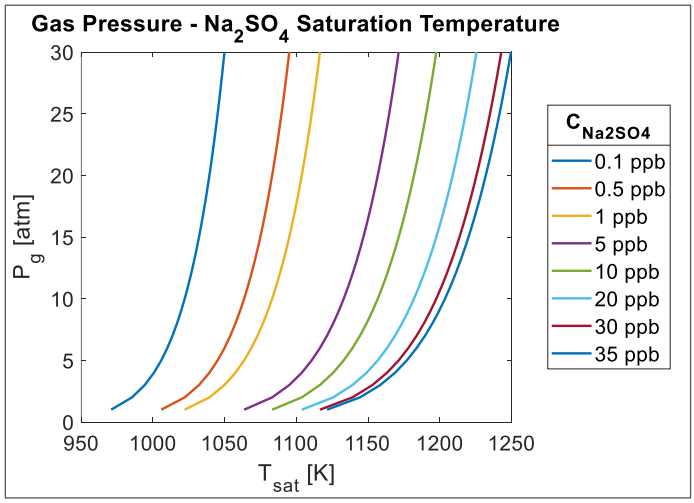

FIGURE 3: SATURATION TEMPERATURE AT DIFFERENT PRESSURES AND SODIUM SULPHATE CONCENTRATIONS

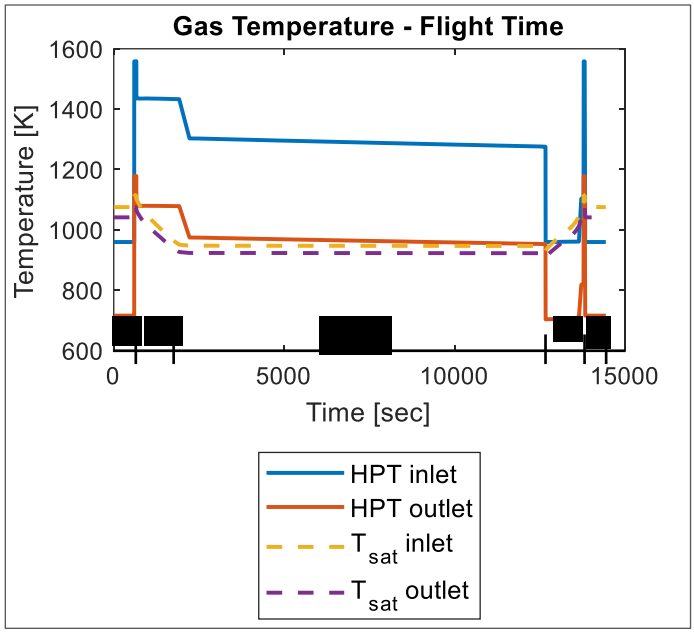

FIGURE 4: SATURATION TEMPERATURE AT INLET AND OUTLET OF THE HPT

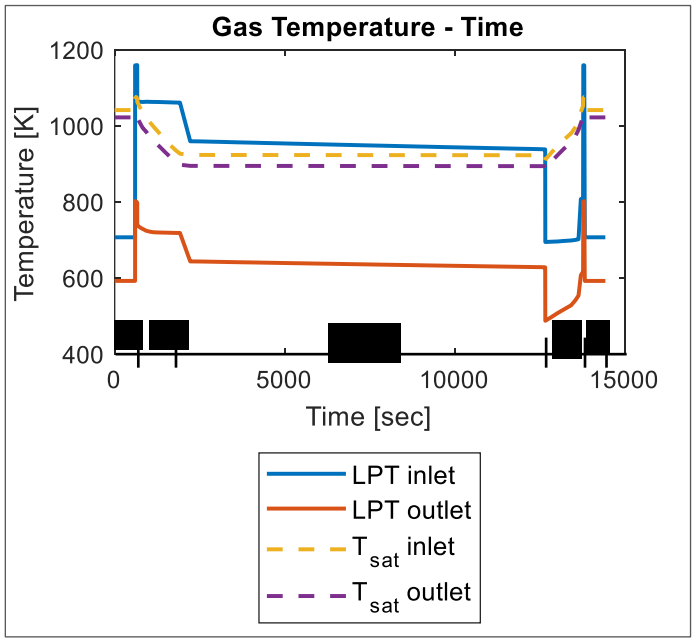

FIGURE 5: SATURATION TEMPERATURE AT INLET AND OUTLET CONDITIONS OF THE LPT

For the calculations in Figure 4 and Figure 5, a sea salt concentration of 8 [ug/m3] at ground level was considered. In Figure 4, it is observed that during take-off, climb, cruise and landing condensation of sodium sulphate is not favored, therefore, the risk for hot corrosion damage is low. The temperature is below the saturation temperature during taxi-in and taxi-out for both inlet and outlet HPT conditions while

during descent only the inlet temperature is above the saturation temperature of sodium sulphate.

From Figure 5 it is deducted that LPT inlet conditions favor evaporation of deposits during take-off, cruise and touch-down at landing. LPT outlet temperatures are too low for hot corrosion to initiate, however, it is expected that some of the intermediate stages fall within the range for condensation. This is a 0-D preliminary assessment of the components in regards to deposition and hot corrosion and a more detailed stage analysis is required to obtain more details about the expected hot corrosion damage in each LPT stage.

ANOVA Tables

Using the normalized Box-Behken design, sets of input parameters were generated based on the design space limits of Table 3. The deposition rate models were inputted with the sets of variables derived by the Box-Behken design and the corresponding model outputs were generated and used in the analysis of variance.

Table 4 and Table 5 present the output of the analysis of variance.

Deposition Rate Model 1		
Source	**F**	**Prob>F**
Na_2SO_4	3.55E+01	1.12E-09
P	32.78091	3.13E-09
V_x	5.115896	0.010387
T_g	0.778983	0.465545
NaCl	6.63E-01	0.520863
T_s	0.002889	0.997116

TABLE 4: ANOVA TABLE FOR DEPOSITION RATE MODEL 1

Deposition Rate Model 2		
Source	**F**	**Prob>F**
P	4.08E+01	1.74E-10
Na_2SO_4	3.26E+01	3.33E-09
V_x	6.49E+00	0.00356
NaCl	3.52E+00	0.038919
T_s	2.109084	0.134324
T_g	0.169292	0.844849

TABLE 5: ANOVA TABLE FOR DEPOSITION RATE MODEL 2

The last column of Table 4 and Table 5 expresses the probability of the variance of the input parameters confirming the null hypothesis [57]. Consequently, the lower the probability, the more important the parameter is identified. ANOVA tables have been sorted based on this probability. Model 1 (Table 4) has higher response to Na_2SO_4 concentration, pressure and gas axial velocity variance. Model 2 (Table 5) is primarily sensitive to pressure, second Na_2SO_4 concentration and third to gas axial velocity.

Sensitivity Analysis comparative figures

Subsequently, sensitivity analysis plots (Figure 6Figure 9) were generated to visualize the response of the two models. In every case, the values of Table 6 were used as constants and one of the parameters T_s, P, T_g, V_x, was varied in each plot.

T_g	1200	[K]
T_s	1000	[K]
P	5	[atm]
V_x	250	[m/s]
C_{NaCl}	5	[ppb]
C_{Na2SO4}	2	[ppb]
L	5	[cm]

TABLE 6: CONSTANT PARAMETERS FOR SENSITIVITY ANALYSIS

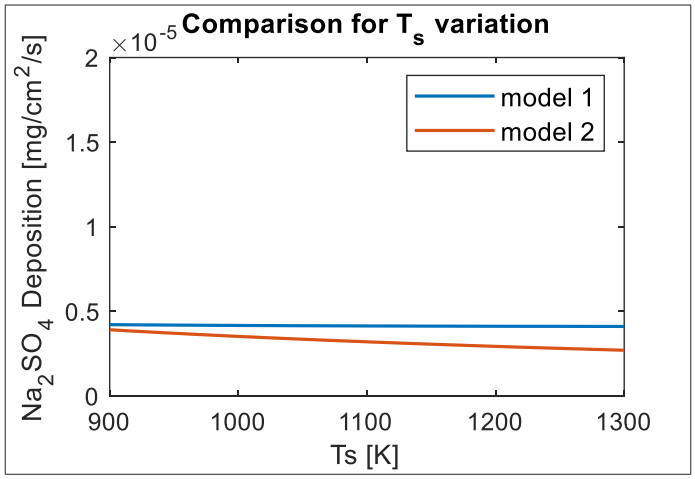

FIGURE 6: SURFACE TEMPERATURE SENSITIVITY ANALYSIS

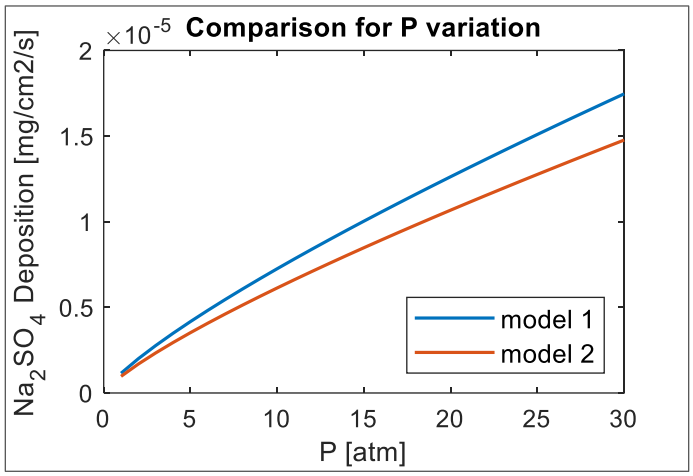

FIGURE 7: PRESSURE SENSITIVITY ANALYSIS

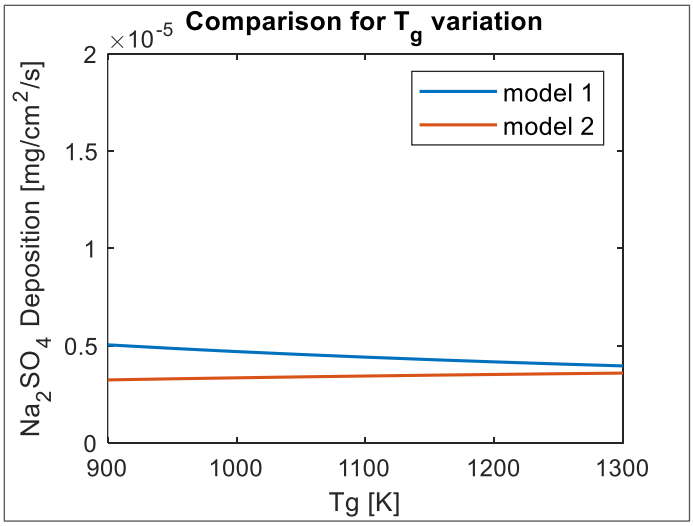

FIGURE 8: GAS TEMPERATURE SENSITIVITY ANALYSIS

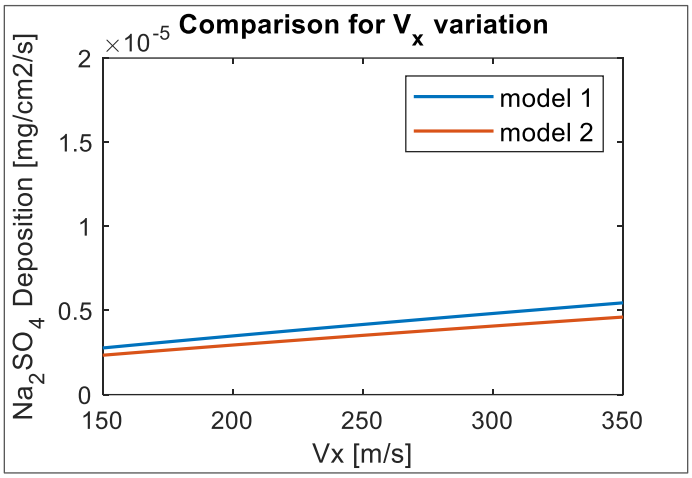

FIGURE 9: AXIAL VELOCITY SENSITIVITY ANALYSIS

Both models agree that an increase in axial velocity (Figure 1) and pressure (Figure 7) increase deposition rate, while higher surface temperature (Figure 6) decreases deposition rate. The biggest difference between the two models is observed in the gas temperature trend (Figure 8). Model 2 suggests that higher gas temperature increases deposition rate while Model 1 suggests the reverse relation. As shown in Equation 1, model 1 is a function of density, which decreases with temperature increase. Mass transfer velocity in model 2 (Equation 3) is a function of Lewis number and Stanton number which are inversely proportional to density and diffusion coefficient, which are increased at higher temperatures. The two models have similar behavior, but model 1 exhibits the ability to capture the fact that at higher temperatures which approach the saturation point, the deposition rate drops. Model 2 also has potential for application but it is advised to be further investigated in combination with evaporation models to account for the fact that at higher temperatures condensation rate decreases.

Discussion

As an outcome of the critical assessment of hot corrosion experimental studies and gas turbine performance analysis, the need for taking into consideration the possible variation of saturation temperature over flight time (Figure 4Figure 5) has been raised. The range for salt condensation and, par extension, for hot corrosion to happen can be altered under the highly varying pressures and environmental exposure levels in real-service conditions. Most material science studies focus on testing the hot corrosion behavior of non-cooled specimens under static air and are disconnected from aircraft-engine-specific conditions and this issue has been addressed in this study.

In regards with the analysis of variance of two deposition rate models, it is cross-validated between the two models that higher pressure and axial velocity increase the deposition rate while higher surface temperature cause a decrease. The only disagreement was observed in the response to gas temperature variation.

However, this trend difference is not a concern since gas temperature is of less importance in both models as derived from the analysis of variance (Table 4,Table 5). Pressure and salt concentration dominate the output of both models. Nevertheless, the absolute numerical differences are of 10^{-6} order of magnitude and it should be noted that in lifing studies the dominant approach is expressing damage relatively since lifing predictions involve high complexity and uncertainty. Performance model errors, microstructural changes, TBC sintering, interaction of different damage mechanisms, changes in the flow and efficiency due to tip leakage increase, fouling or erosion are some of the reasons that induce high uncertainty and complexity in lifing predictions. In this context, the numerical values and responses of the two models under investigation were found to be comparable.

CONCLUSION

The analysis of variance for two sodium sulphate deposition rate models in literature has been presented. There are similarities in the trends of the models' behavior and the observed differences have been identified and discussed. The most dominant parameters that increase the deposition rate are pressure and salt concentration in the gas flow. For the purposes of aircraft engine lifing investigations for hot corrosion damage, such models have good applicability as they correlate gas turbine operational parameters with the deposition rate per surface and time, without going into particle level detail. In addition, the variation of sodium sulphate saturation point has been considered under different operating conditions. Higher salt concentration and higher pressure increase the saturation point which means condensation can continue up to higher temperatures.

This study is part of a research on hot corrosion damage prediction in aircraft engines. The application of the deposition rate models under investigation is integrated with a framework combining models which deal with different aspects of hot corrosion mechanism. As a future direction, the calculation of deposition rate at different components in-flight is proposed with

application of analytical models in order to make use of hot corrosion rate experimental models and experimental data developed in controlled lab conditions.

In summary, the novel concepts that were introduced in this work are:

- Identifying and reflecting upon the gaps between superalloy hot corrosion testing and aircraft engine real-service conditions which are highly varying and involve both cooled and non-cooled surfaces.
- Incorporating a saturation point investigation, based on operating pressure and environmental exposure level in the flight mission analysis in order to investigate the possibility of evaporation mechanisms coming into effect.
- Analysis of variance and sensitivity analysis of two deposition rate models which are proposed as feasible for integration in a hot corrosion study in aircraft engines. Their response and behavior were compared and their differences were identified in order to be used in a hot corrosion study.
- Knowledge of material science, gas turbine performance analysis, environmental data and deposition rate models were combined to set the basis for a new approach in the currently unexplored area of hot corrosion damage estimation in aircraft engines.

ACKNOWLEDGMENTS

This study is part of a research project supported by Lufthansa Technik.

REFERENCES

[1] Wood, M. I., 2000, "Gas Turbine Hot Section Components: The Challenge of 'residual Life' Assessment," Proc. Inst. Mech. Eng. Part A J. Power Energy, **214**(3), pp. 193–201.

[2] Haslam, A., Abu, A., Laskaridis, P., and Access, O., 2015, "A Method for the Assessment of Operational Severity for a High Pressure Turbine Blade of an Aero-Engine Thermo-Mechanical Fatigue Model," pp. 447–456.

[3] Abu, A. O., Eshati, S., Laskaridis, P., and Singh, R., 2014, "Aero-Engine Turbine Blade Life Assessment Using the Neu/Sehitoglu Damage Model," Int. J. Fatigue, **61**, pp. 160–169.

[4] Rezazadeh Reyhani, M., Alizadeh, M., Fathi, A., and Khaledi, H., 2013, "Turbine Blade Temperature Calculation and Life Estimation - a Sensitivity Analysis," Propuls. Power Res., **2**(2), pp. 148–161.

[5] Ghafir, M. F. A., and Wang, L., 2018, "Creep Life Prediction for Aero Gas Turbine Hot Section Component Using Artificial Neural Networks," **136**(March 2014), pp. 1–9.

[6] Hanumanthan, H., Stitt, A., Laskaridis, P., and Singh, R., 2011, "Severity Estimation and Effect of Operational Parameters for Civil Aircraft Jet Engines," **226**, pp. 1544–1561.

[7] Larhga, J. S., and Kumar, D., 2016, *Final Report of Serious Incident Involving M/s Jet Airways ATR 72-500 Aircraft VT-JCL AT Bangalore on 15/06/2016*.

[8] Australian Transport Safety Bureau, 2008, *In-Flight Engine Malfunction and Air Turn-Back, 240 Km W Darwin NT, 24 September 2006, VH-TJI, Boeing Co. 737-476*, Canberra, Australia.

[9] Homaeian, A., and Alizadeh, M., 2016, "Interaction of Hot Corrosion and Creep in Alloy 617," EFA, **66**, pp. 373–384.

[10] Lortrakul, P., Trice, R. W., Trumble, K. P., and Dayananda, M. A., 2014, "Investigation of the Mechanisms of Type-II Hot Corrosion of Superalloy CMSX-4," Corros. Sci., **80**, pp. 408–415.

[11] Shifler, D. A., 2018, "Hot Corrosion: A Modification of Reactants Causing Degradation," Mater. High Temp., **35**(1–3), pp. 225–235.

[12] Bose, S., 2018, "Field and Simulated Field Experience," *High Temperature Coatings*, pp. 327–357.

[13] Simms, N. J., Heikinheimo, L., Encinas-Oropesa, A., Tuurna, S., Kilgallon, P. J., Nicholls, J. R., and Oakey, J. E., "Volume 6 Paper H046 Predicting Type II Hot Corrosion in Industrial Gas Turbines," **6**, pp. 1–25.

[14] Sumner, J., Encinas-Oropesa, A., Simms, N. J., and Nicholls, J. R., 2013, "Type II Hot Corrosion: Kinetics Studies of CMSX-4," Oxid. Met., **80**(5–6), pp. 553–563.

[15] Nicholls, J. R., Simms, N. J., and Encinas-Oropesa, A., 2007, "Modelling Hot Corrosion in Industrial Gas Turbines," Mater. High Temp., **24**(3), pp. 149–162.

[16] Mei, H., Liu, Y., Cheng, L., and Zhang, L., 2012, "Corrosion Mechanism of a NiCoCrAlTaY Coated Mar-M247 Superalloy in Molten Salt Vapour," Corros. Sci., **55**, pp. 201–204.

[17] Sreedhar, G., and Raja, V. S., 2010, "Hot Corrosion of YSZ / Al 2 O 3 Dispersed NiCrAlY Plasma-Sprayed Coatings in Na 2 SO 4 – 10 Wt .% NaCl Melt," Corros. Sci., **52**(8), pp. 2592–2602.

[18] Ahluwalia, R. K., 1988, "Correlation Between Sodium Sulfate Mass Transfer and Low-Temperature Hot Corrosion," ASME 88-GT.

[19] Sumner, J., Potter, A., Simms, N. J., and Oakey, J. E., 2015, "Hot Corrosion Resistance of Gas Turbine Materials in Combusted Syngas Environments," Mater. High Temp., **32**(1–2), pp. 177–187.

[20] Corrosion, H. T., 2007, "Hot Corrosion in Gas Turbines," High Temp. Corros. Mater. Appl., pp. 249–258.

[21] Bose, S., 2007, "Chapter 5 - High-Temperature Corrosion," *High-Temperature Corrosion*, pp. 53–70.

[22] Kalsi, S. S., 2016, "Hot Corrosion and Its Mechanism: A Review," **7**(1), pp. 133–136.

[23] Sahu, J. K., Ravi Kumar, B., Das, S. K., Paulose, N., and Mannan, S. L., 2015, "Isothermal High Temperature Low Cycle Fatigue Behavior of Nimonic-263: Influence of Type I and Type II Hot Corrosion," Mater. Sci. Eng. A, **622**(January), pp. 131–138.

[24] Rapp, R. A., 2002, "Hot Corrosion of Materials: A Fluxing Mechanism?," Corros. Sci., **44**(2), pp. 209–221.

[25] Agarwal, N., and Khan, E., 2018, “OXIDATION AND CORROSION BEHAVIOUR OF INCONEL-600 IN AIR AND SALT AT 800 0 C IN 50 CYCLIC CONDITION.”
[26] Simms, N. J., Encinas-Oropesa, A., and Nicholls, J. R., 2008, “Modelling the Development of Type I Hot Corrosion on Coated and Uncoated Single Crystal Superalloys,” Mater. Sci. Forum, **595**–**598**, pp. 689–698.
[27] Bose, S., 2007, *High Temperature Coatings*.
[28] Bornstein, N. S., and Decrescente, M. A., 2018, “Deposition — Hot Corrosion in Gas Turbine Engines,” pp. 2–5.
[29] Eliaz, N., Shemesh, G., and Latanision, R. M., 2002, “Hot Corrosion in Gas Turbine Components,” Eng. Fail. Anal., **9**(1), pp. 31–43.
[30] Sequeira, C. A. C., 2003, “Hot Corrosion in Gas Turbines,” Molten Salt Forum, **7**, pp. 85–104.
[31] Pettit, F., 2011, “Hot Corrosion of Metals and Alloys,” Oxid. Met., **76**(1–2), pp. 1–21.
[32] Eriksson, R., Brodin, H., Johansson, S., Östergren, L., and Li, X.-H., 2013, “Cyclic Hot Corrosion of Thermal Barrier Coatings and Overlay Coatings,” Proc. ASME Turbo Expo 2013, p. V004T02A009.
[33] Simms, N. J., Encinas-Oropesa, A., and Nicholls, J. R., 2008, “Hot Corrosion of Coated and Uncoated Single Crystal Gas Turbine Materials,” Mater. Corros., **59**(6), pp. 476–483.
[34] Deodeshmukh, V. P., 2015, “Evaluating the Hot Corrosion Behavior of High-Temperature Alloys for Gas Turbine Engine Components,” Jom, **67**(11), pp. 2608–2614.
[35] Kotsiopoulos, P., 2005, “An Integrated Engine - Aircraft Perfomance Platform for Assessing New Technologies in Aeronautics,” pp. 1–13.
[36] Borello, D., Angeli, L. D., Salvagni, A., Venturini, P., Rispoli, F., Meccanica, I., and Università, S., 2018, “GT2014-26250 STUDY OF PARTICLES DEPOSITION IN GAS TURBINE BLADES IN PRESENCE OF,” pp. 1–12.
[37] Guha, A., 2008, “Transport and Deposition of Particles in Turbulent and Laminar Flow,” Annu. Rev. Fluid Mech., **40**(1), pp. 311–341.
[38] Soldati, A., and Marchioli, C., 2009, “Physics and Modelling of Turbulent Particle Deposition and Entrainment: Review of a Systematic Study,” Int. J. Multiph. Flow, **35**(9), pp. 827–839.
[39] Forsyth, P., Gillespie, D. R. H., Mcgilvray, M., and Mead, O., 2018, “DYNAMIC MESH MORPHING APPROACH FOR THE NUMERICAL SIMULATION OF,” pp. 1–15.
[40] Bons, J. P., Prenter, R., and Whitaker, S., 2017, “A Simple Physics-Based Model for Particle Rebound and Deposition in Turbomachinery,” J. Turbomach., **139**(8), p. 081009.
[41] Rosner, D. E., Chen, B.-K., Fryburg, G. C., and Kohl, F. J., 1979, “Chemically Frozen Multicomponent Boundary Layer Theory of Salt and/or Ash Deposition Rates from Combustion Gases,” Combust. Sci. Technol., **20**(3–4), pp. 87–106.
[42] Helt, J. E., 1980, *Evaluation of Alkali Metal Sulphate Dew Point Measurement for Detection of Hot Corrosion Conditions in PFBC Flue Gas*, Argonne, Illinois.
[43] Sun, D., Xu, J., and Chen, Q., 2014, “Modeling of the Evaporation and Condensation Phase-Change Problems with FLUENT,” Numer. Heat Transf. Part B Fundam., **66**(4), pp. 326–342.
[44] Rosner, D., 1994, “Transport Phenomena and Interfacial Kinetics in Multiphase Combustion Systems.”
[45] Rosner, E., *Turbine Airfoil Deposition Models*.
[46] Santoro, G. J., Gokoglu, S. A., Kohl, F. J., Stearns, C. A., and Rosner, D. A., 1985, “DEPOSITION OF Na<inf>2</Inf>SO<inf>4</Inf> FROM SALT-SEEDED COMBUSTION GASES OF A HIGH VELOCITY BURNER RIG.,” AIME, Metall. Soc, pp. 417–434.
[47] Rosner, D. E., 1978, “THERMAL (SORET) DIFFUSION EFFECTS ON INTERFACIAL MASS TRANSPORT RATES.,” PCH. Physicochem. Hydrodyn., **1**(2–3), pp. 159–185.
[48] Jeong, K., Kessen, M. J., Bilirgen, H., and Levy, E. K., 2010, “Analytical Modeling of Water Condensation in Condensing Heat Exchanger,” Int. J. Heat Mass Transf., **53**(11–12), pp. 2361–2368.
[49] Hallet, J. C., and Stern, K. H., 1980, *No Title*.
[50] NIST, “Sodium Sulphate” [Online]. Available: https://webbook.nist.gov/cgi/cbook.cgi?ID=C7757826&Mask=4#Thermo-Phase. [Accessed: 18-Nov-2019].
[51] Wisniak, J., 2001, “Historical Development of the Vapor Pressure Equation from Dalton to Antoine,” J. Phase Equilibria, **22**(6), pp. 622–630.
[52] Ferreira, S. L. C., Bruns, R. E., Ferreira, H. S., Matos, G. D., David, J. M., Brandão, G. C., da Silva, E. G. P., Portugal, L. A., dos Reis, P. S., Souza, A. S., and dos Santos, W. N. L., 2007, “Box-Behnken Design: An Alternative for the Optimization of Analytical Methods,” Anal. Chim. Acta, **597**(2), pp. 179–186.
[53] Rihan, R., Shawabkeh, R., and Al-Bakr, N., 2014, “The Effect of Two Amine-Based Corrosion Inhibitors in Improving the Corrosion Resistance of Carbon Steel in Sea Water,” J. Mater. Eng. Perform., **23**(3), pp. 693–699.
[54] Prospero, J. M., 1979, “Mineral and Sea Salt Aerosol Concentrations in Various Ocean Regions,” J. Geophys. Res., **84**(C2), p. 725.
[55] Montgomery, D. C., *Design and Analysis of Experiments*, John Wiley & Sons.
[56] The MathWorks Inc, “MATLAB 2019b.”
[57] Sawyer, S. F., 2009, “Analysis of Variance: The Fundamental Concepts,” J. Man. Manip. Ther., **17**(2), pp. 27E-38E.
[58] National Institute of Standards and Technology, U. D. of C., “NIST Chemistry WebBook, SDR 69” [Online]. Available:

https://webbook.nist.gov/cgi/cbook.cgi?ID=C7757826&Mask=4&Type=ANTOINE&Plot=on. [Accessed: 20-Sep-2009].

[59] Bogatyrev, A. F., Makeenkova, O. A., Belalov, V. R., and Kucherenko, M. A., 2017, "Calculation of Viscosity and Diffusion Coefficients in Binary Mixtures of Dilute Gases," Adv. Stud. Theor. Phys., **11**(6), pp. 283–296.

[60] Ghiaasiaan, S. M., 1954, "Collision Integrals for the Lennard-Jones Potential Model," *Convective Heat and Mass Transfer*, Cambridge University Press, p. 5756.

APPENDIX

Antoine Parameters

Antoine Parameters for sodium sulphate evaporation [58]:
A: 1.93334
B: 7517.522
C: -375.044

Gas Diffusion Coefficient [42,59]

$$D = \frac{0.001853 \cdot T\sqrt{T \cdot \left(\frac{1}{MW_A} + \frac{1}{MW_B}\right)}}{P \cdot \sigma_{AB}^2 \cdot \Omega_{D,AB}}$$

Collision Integrals for the Lennard-Jones Potential Model obtained from [60].

3^k Box-Behnken Factorial Design (normalized)

Var 1	Var 2	Var 3	Var 4	Var 5	Var 6
-1	-1	0	-1	0	0
-1	-1	0	1	0	0
-1	1	0	-1	0	0
-1	1	0	1	0	0
1	-1	0	-1	0	0
1	-1	0	1	0	0
1	1	0	-1	0	0
1	1	0	1	0	0
0	-1	-1	0	-1	0
0	-1	-1	0	1	0
0	-1	1	0	-1	0
0	-1	1	0	1	0
0	1	-1	0	-1	0
0	1	-1	0	1	0
0	1	1	0	-1	0
0	1	1	0	1	0
0	0	-1	-1	0	-1
0	0	-1	-1	0	1
0	0	-1	1	0	-1
0	0	-1	1	0	1
0	0	1	-1	0	-1
0	0	1	-1	0	1
0	0	1	1	0	-1
0	0	1	1	0	1
-1	0	0	-1	-1	0
-1	0	0	-1	1	0
-1	0	0	1	-1	0
-1	0	0	1	1	0
1	0	0	-1	-1	0
1	0	0	-1	1	0
1	0	0	1	-1	0
1	0	0	1	1	0
0	-1	0	0	-1	-1
0	-1	0	0	-1	1
0	-1	0	0	1	-1
0	-1	0	0	1	1
0	1	0	0	-1	-1

0	1	0	0	-1	1
0	1	0	0	1	-1
0	1	0	0	1	1
-1	0	-1	0	0	-1
-1	0	-1	0	0	1
-1	0	1	0	0	-1
-1	0	1	0	0	1
1	0	-1	0	0	-1
1	0	-1	0	0	1
1	0	1	0	0	-1
1	0	1	0	0	1
0	0	0	0	0	0
0	0	0	0	0	0
0	0	0	0	0	0
0	0	0	0	0	0
0	0	0	0	0	0
0	0	0	0	0	0

Comparison of sodium sulphate deposition rate models based on operational factors influencing hot corrosion damage in aero-engines

Pontika, Evangelia

2021-01-11

Pontika E, Laskaridis P, Nikolaidis T, Koster M. (2021) Comparison of sodium sulphate deposition rate models based on operational factors influencing hot corrosion damage in aero-engines. In: ASME Turbo Expo 2020: Turbomachinery Technical Conference and Exposition (GT2020), 21-25 September 2020, London, Virtual Event

https://doi.org/10.1115/GT2020-15715